Ionization and recombination rates for highly ionized titanium ions from time-resolved spectroscopy of tokamak plasmas

Jieh-Shan Wang, Hans R. Griem, and Roger Hess
Laboratory for Plasma and Fusion Energy Studies, University of Maryland, College Park, Maryland 20742

William L. Rowan and Thaddeus P. Kochanski
Fusion Research Center, The University of Texas, Austin, Texas 78712
(Received 2 August 1985)

The effective ionization and recombination rate coefficients for Ti XVII–XX were obtained by studying the modulation of line emission by sawtooth oscillations in the TEXT tokamak at the University of Texas. Experimental data are matched with the simulation of titanium-ion emission by a one-dimensional (1D) transport code which includes ionization and recombination processes. The rate coefficients were determined for $T_e \approx 600-1100$ eV and $N_e \sim 4\times 10^{13}$ cm^{-3}. The ionization rates were about 20% higher than values calculated by Lotz's formula. The recombination rates were about 20% less than theoretical values. The uncertainty of ionization and recombination rate coefficients is estimated to be less than 20% and 60%, respectively. The sensitivity of our method to various parameters, i.e., the diffusion coefficient, convective velocity, and electron temperature, is also discussed.

I. INTRODUCTION

The study of the transport of impurities and the calculation of the power balance in a fusion plasma require accurate atomic data such as ionization and recombination rate coefficients. Measurements of atomic rate coefficients have previously been made on Θ pinches which produce plasmas that can be well diagnosed.[1–3] However, most of the highly ionized atoms appearing in fusion plasmas cannot be studied in such short-lived and low-T_e devices. They can only be studied in the high-temperature plasma devices, i.e., tokamaks, where they appear as natural impurities or are introduced artificially. Breton *et al.*[4] observed the sawtooth modulation of Mo XXXI and XXXII line emissions in a tokamak plasma and determined the ionization and recombination rates for Mo XXXI to within a factor of 2. The ratios of ionization to recombination rate coefficients for Fe XV–XIX were measured by Isler *et al.*[5] during the counterinjection of neutral beams into the ISX-*B* tokamak at Oak Ridge National Laboratory. However, in a tokamak plasma, transport of particles strongly affects the behavior of impurities in the plasma. It is difficult to separate transport processes from atomic processes in the study of spectral line emission of impurity ions. Therefore, one can obtain the atomic rate coefficients only when the transport processes can be sufficiently discounted or taken into account. Breton *et al.*[4] neglected the transport effect by assuming Mo XXXI and XXXII are concentrated in the center of the plasma. Isler *et al.*[5] assumed that the iron ions can reach coronal equilibrium because the equilibration time is much shorter than the observed ion-confinement time during the neutral-beam counterinjection. The dielectronic recombination rate coefficients, relative to excitation rate coefficients, have also been obtained for heliumlike calcium Ca XIX (Ref. 6) and iron Fe XXV (Ref. 7) and hydrogenlike Ti XXII (Ref. 8) from measurements of satellite to resonance line ratios.

This paper describes the determination of ionization and recombination rates for highly ionized titanium ions. Titanium can be the dominant high-Z impurity in tokamaks with titanium-carbide-coated limiters or parts containing titanium. Sawtooth modulation of line emission from titanium ions in a tokamak plasma was analyzed using the technique of Breton *et al.*,[4] modified to allow for impurity transport and radial variations. A one-dimensional transport-ionization-recombination code was used to simulate the behavior of titanium ions. With the rate coefficients as adjustable parameters, the simulated and observed time histories of titanium-ion lines were matched. The accuracy of this method for determining the rate coefficients and the effect of transport due to diffusion and convection will also be discussed.

The principle of the method and experimental considerations are discussed in the following section. The numerical code and its input parameters are described in Sec. IV. Section V summarizes the procedures and results of the study. The sensitivity of the method is discussed in Sec. VI, as are the possible effects of transport and uncertainties from errors in the electron temperature and density.

II. PRINCIPLE OF THE MEASUREMENT

Sawtooth oscillations on soft-x-ray signals from the central region of a tokamak plasma have been observed extensively since 1974.[9–12] These oscillations have also been observed on other diagnostics including line radiation from highly ionized impurities,[4,13,14] central temperature, and chord-averaged electron density. The TFR group[15] reported that the majority of the sawtooth oscillation was due to variations in the central electron temperature while the electron density was little changed. They found that the central electron density varied by 1–4%

with a corresponding variation of 10—15 % in the central electron temperature. Thus, for typical conditions the variation in electron density during a sawtooth can be considered to be a minor contributor to the ionization-recombination equilibrium.

The ionization-recombination equilibrium of impurity ions varies as the electron temperature fluctuates. The variations of abundances of these ions can be observed in the modulation of line emissions. Effective ionization and recombination rates for these ions may therefore be obtained by studying the relation between the modulation of the line emissions and the electron temperature fluctuations or between the line emission modulation and the sawtooth oscillations of the soft-x-ray signals.

For optically thin resonance lines of the impurity ions in a low-density plasma, the line intensity can be described by the coronal formula[16]

$$L=\int \frac{h\nu}{4\pi} n_e n_g X\, dr \ , \tag{1}$$

where n_e is the electron density, n_g is the impurity ion density in the ground state, X is the excitation rate coefficient, and the integration is along the line of sight of the spectrometer. Since the electron density can be considered to be constant and the excitation rate coefficient is a very slowly varying function of T_e when T_e is well above the threshold excitation energy, only the variation of n_g is reflected in the observed line signal.

The electron collisional excitation rates were calculated for Ti-ion lines from the theoretical data given by Bahtia *et al.*[17] The excitation rate of resonance lines at $T_e=900$ eV varies less than 3% for a change in T_e of 50 eV. The ratio of ionization to recombination rates calculated from semiempirical formulas of Lotz[18] and Burgess[19] (see Sec. IV), however, varies more than 15%.

For forbidden lines from transitions between levels of the ground configuration of the impurity ions, one has to consider how the population equilibrium is established between these levels. The forbidden line intensity is

$$\begin{aligned} L&=\int \frac{h\nu}{4\pi} A n_u dr \\ &=\int \frac{h\nu}{4\pi} A a_u n_g dr \ , \end{aligned} \tag{2}$$

where A is the transition probability, and a_u is the fractional abundance of the upper level. As T_e varies, both a_u and n_g will change. As the change of n_g is governed essentially by the ionization and recombination processes, the repopulation of the upper level for the forbidden line is governed by excitation and deexcitation processes. The excitation and deexcitation are from electron or proton collisions and radiative transitions.[17] The electron collisional excitation rates for the ground levels at $T_e=900$ eV vary less than 7% for a change in T_e of 50 eV. However, since collisional deexcitation rates are essentially proportional to the collisional excitation rates, the fractional abundance a_u will change by much less than 7%. Thus, the modulation in the forbidden line intensity is also mostly due to the variation in ionic abundances.

The relaxation time τ_r for ionic abundances to reach equilibrium at constant T_e has to be considered in the analysis. For the modulation of the abundance of ions to be significant as T_e fluctuates, τ_r has to be comparable to the sawtooth period τ_s. If $\tau_r \gg \tau_s$, then the response of the ionization-recombination process cannot follow the temperature fluctuations, and there will not be any change in the ionic abundances. If $\tau_r \ll \tau_s$, the change of ionic abundance will closely follow that of the electron temperature. In this case, the line emission signal will be exactly in phase or out of phase with the soft-x-ray signal from the same plasma region. In such a case the ionization and recombination rates cannot be obtained either, because any differences in the rates are not reflected in the line emission signals. A preliminary estimate from rates calculated by the semiempirical formulas gives τ_r of about 2—8 ms. This is comparable with the sawtooth period of 3—5 ms in these experiments.

The abundance of impurity ions in a tokamak plasma is calculated here by solving the one-dimensional (1D) impurity transport-ionization-recombination equation in cylindrical coordinates

$$\begin{aligned} \frac{\partial n_k}{\partial t} &= -\frac{1}{r}\frac{\partial}{\partial r}(r\Gamma_k) \\ &\quad + n_e(I_{k-1}n_{k-1} - I_k n_k - R_k n_k + R_{k+1}n_{k+1}) \ , \end{aligned} \tag{3}$$

where the Γ_k are the particle fluxes, the I_k's are the ionization rate coefficients, and the R_k's are the recombination rate coefficients. The particles fluxes are written as

$$\Gamma_k = -\left[D(r)\frac{\partial n_k}{\partial r} + V(r) n_k \right] , \tag{4}$$

where $D(r)$ is the diffusion coefficient and $V(r)$ is the convective velocity, both assumed to be independent of the ionization stage k.

To solve the equations, the diffusion coefficient, the convective velocity, and the ionization and recombination rates are needed. If these parameters have no time dependence, an equilibrium can be achieved. If any parameters have a time dependence of the form $P(t)=P_0 + P_1\exp(i2\pi t/\tau_s)$, then the solution in the first approximation should be of the form

$$n_k(r,t)=n_k^0(r)+n_k^1(r)\exp\left[i2\pi \left[\frac{t}{\tau_s} - \theta_k(r) \right] \right] . \tag{5}$$

$n_k^0(r)$ is the solution of Eq. (3) when $\partial n_k/\partial t=0$. The phase shift $\theta_k(r)$ will depend on the values of the various parameters. In this experiment, the ionization and recombination rate coefficients have a time dependence corresponding to the sawtooth oscillations and, therefore, the solutions of the equations will vary with a period τ_s.

Correlation functions[20]

$$C_k(\tau)=\frac{\int_0^T S(t)L_k(t+\tau)dt}{|S|\ |L_k|} \tag{6}$$

are calculated from the solution of the equations. Here,

$$L_k(t) = \int_0^a n_k(r,t) n_e(r) X_k(r) dr \quad \text{for resonance lines}$$
$$= \int_0^a n_k(r,t) dr \quad \text{for forbidden lines},$$

$S(t)$ is a sawtooth function corresponding to the sawtooth oscillation in the experiment, and $X_k(r)$ is the excitation rate coefficient. The normalization factors $|S|$ and $|L_k|$ are defined as

$$|S| = \left[\int_0^T S(t) S(t) dt \right]^{1/2}$$

and

$$|L_k| = \left[\int_0^T L_k(t) L_k(t) dt \right]^{1/2}.$$

The integration of the ion densities n_k over the plasma radius is performed for consistency with the experiment in which the monochromators view the plasma along the central chord. However, the ions of interest are mostly at radii less than 15 cm. The $C_k(\tau)$ are compared with the experimental correlation functions (see next section). The rate coefficients are then adjusted to improve the correlations. This procedure is iterated until the best match of theory and experiment is obtained.

We must note that the ionic abundances and line emissions described by Eqs. (1) and (2) might be affected by transport processes. The time scale for usual transport in a tokamak, i.e., the impurity confinement time, is much larger than the sawtooth period. Therefore, the effects of transport are less important, except possibly for anomalous transport during the sawtooth crash phase. Such effects have been observed in several tokamak experiments. Petrasso *et al.*[21] observed flattening of Si XV, XIV, and XIII profiles after the sawtooth crash in the Alcator-*C* tokamak at the Massachusetts Institute of Technology. This may be explained by an increase in the diffusion coefficient. The TFR group[22] observed fast expulsion of Ni ions out of the $q=1$ surface in a neutral-beam-heated deuterium plasma during the sawtooth crash. They explain this by assuming an outward convection of the ions. However, we do not have such clear evidence that sufficiently rapid transport phenomena exist in the TEXT tokamak, at least not for the conditions we have studied. For these conditions the transport coefficients can be assumed constant and be determined by the impurity injection technique.[23] Any rapid transport would cause modulations in the line emissions either in phase or 180° out of phase with the sawtooth oscillation. In contrast, we have observed gradual changes of phase from ion to ion (see next section). We suggest some of these differences are due to neutral-beam heating[22] or due to a much higher ohmic-heating power density[21] than in the present experiments.

III. THE EXPERIMENT

The measurements of the Ti rate coefficients were made on the TEXT tokamak.[24] TEXT is a medium-sized, ohmically heated tokamak with a major radius of 100 cm and a minor radius of 27 cm. After a 40-msec current rise period, the discharge settles down to a quiescent state with constant parameters which lasts for 300—400 ms. The toroidal magnetic field can be varied over a range of 10—30 kG. Plasma currents have been obtained from 100 to 450 kA with both constant and ramping currents. The shot-to-shot reproducibility of the macroscopic parameters, the central electron temperature, and central-chord-averaged electron density is good with less than 10% variation. We studied three plasma conditions. The toroidal magnetic fields, plasma currents, and other parameters for the three conditions are listed in Table I.

Fluctuations in the soft-x-ray emission were studied with the TEXT silicon surface barrier array.[25] The array consists of 40 diodes with spatial resolution of 1.1 cm over 80% of the plasma. The data were digitized at 20 kHz with eight-bit digitizers. The minimum detectable level of fluctuations normalized to the quiescent period signal is 0.5%.

During the experimental period, a typical discharge exhibited soft-x-ray signals with an 18—20% modulation and a period of 3—5 ms. The period of a sawtooth is proportional to the density[25] and therefore varies somewhat during a single discharge. The sawteeth invert at a radius which is consistent with the $q=1$ radius calculated with the temperature profile measured by Thomson scattering and assuming Spitzer conductivity.

The spectral lines observed are listed in Table II. The instruments employed were a 2.2-m grazing-incidence (GI) monochromator, a 1-m normal-incidence (NI) monochromator, and a 1-m Czerny-Turner (CT) monochromator. Each of these viewed a central plasma chord in the plasma midplane.

Figure 1(a) shows the time-resolved signals of central-cord soft-x-ray Ti XVII 3834 Å, Ti XVIII 1778 Å, Ti XIX 2345 Å, and Ti XX 309 Å lines for case I. Figures 2(a) and 3(a) show the soft-x-ray and spectral line signals for cases II and III, respectively. The spectral line signals, at first glance, do no appear to be correlated with the soft-x-ray signal. This is mostly due to the high noise level in

TABLE I. Plasma conditions.

Case	Plasma current (kA)	Toroidal magnetic field (kG)	Central electron temperature (eV)	Chord-averaged electron density (10^{13} cm^3)	b[a] (cm)	c[a]
I	300	28	900	3.5	16.1	2.52
II	400	28	1100	4.2	18.4	3.7
III	200	20	600	3.5	16.9	2.7

[a] b and c are parameters for electron temperature profiles as discussed in the text.

TABLE II. Lines used for cross correlations with soft-x-ray signals (Refs. 26–28).

Ion	Transition	Wavelength (Å)	Monochromator
Ti XX	$2p(^2P_{3/2})$-$2s(^2S_{1/2})$	259.30	2.2-m GI
Ti XX	$2p(^2P_{1/2})$-$2s(^2S_{1/2})$	309.09	2.2-m GI
TI XIX	$2s2p(^1P_1)$-$2s^2(^1S_0)$	169.59	2.2-m GI
Ti XIX	$2s2p(^3P_1)$-$2s^2(^1S_0)$	328.34	2.2-m GI
Ti XIX	$2s2p(^3P_1)$-$2s2p(^3P_2)$	2345.00	1.0-m CT
Ti XVIII	$2p(^2P_{3/2})$-$2p(^2P_{1/2})$	1777.95	1.0-m NI
Ti XVII	$2p^2(^3D_2)$-$2p^2(^3D_1)$	3834.6	1.0-m CT
Ti XVII	$2p^2(^3D_1)$-$2p^2(^3D_0)$	3371.6	1.0-m CT

the signals. In order to extract the relation between the signals we calculated the cross correlation of the signals. The signals are processed by a digital filter routine with band pass 100–2000 Hz.[29] The dc level and high-frequency noise of the signal are eliminated by the filtering process.

The correlation functions were again calculated from Eq. (6) for $0 \le \tau \le t_s$, where $S(t)$ and $L_k(t)$ are now the filtered soft-x-ray and line emission signals, respectively. The time T is chosen to span several sawtooth oscillations, and t_s is the sawtooth period. In practice, the correlations were calculated by the method of fast Fourier transforms. The frequency spectra of the signals were obtained from the Fourier transforms. Then the autopower or cross-power spectra were calculated from the multiplication of the complex conjugate of one spectrum with the same or other spectra. The power spectra were then back-transformed to become the correlations. The statistics of the calculation improve with the number of sawtooth periods contained in the interval. However, primarily due to density variations, the sawtooth periods change even during a single shot. Therefore, we used only time spans that contain sawtooth cycles of similar periods. Figure 1(b) shows the cross correlations of Ti XVII 3834 Å, Ti XVIII 1778 Å, Ti XIX 2345 Å, and Ti XX 309 Å lines with the soft-x-ray signal for case I. The phase shift θ was directly obtained from the power spectra. Cross correlations for cases II and III are shown in Figs. 2(b) and 3(b).

If the light emissions were independent of the soft-x-ray signal, the cross correlations would be approximately zero. Figure 4 shows the correlations of continuum radiation

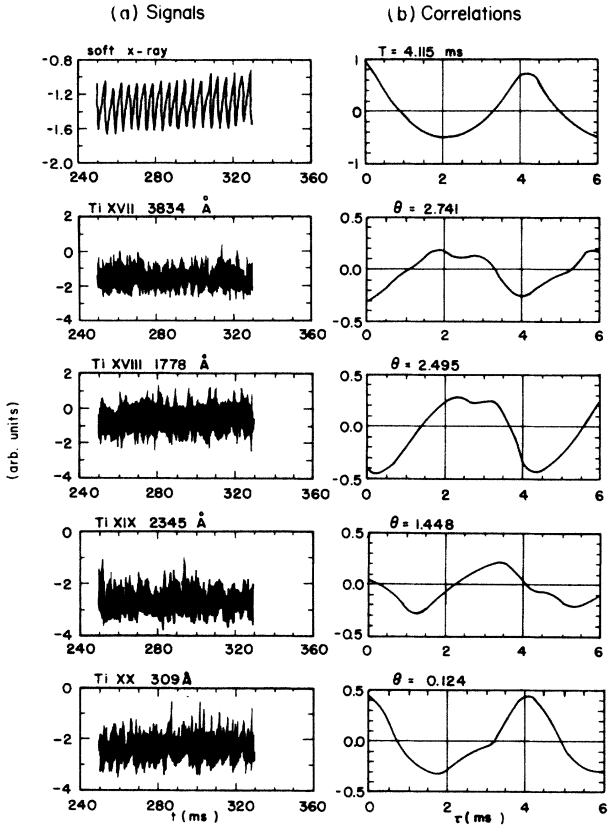

FIG. 1. Signals and correlations for case I. T is the averaged sawtooth period and θ is the phase shift in rad.

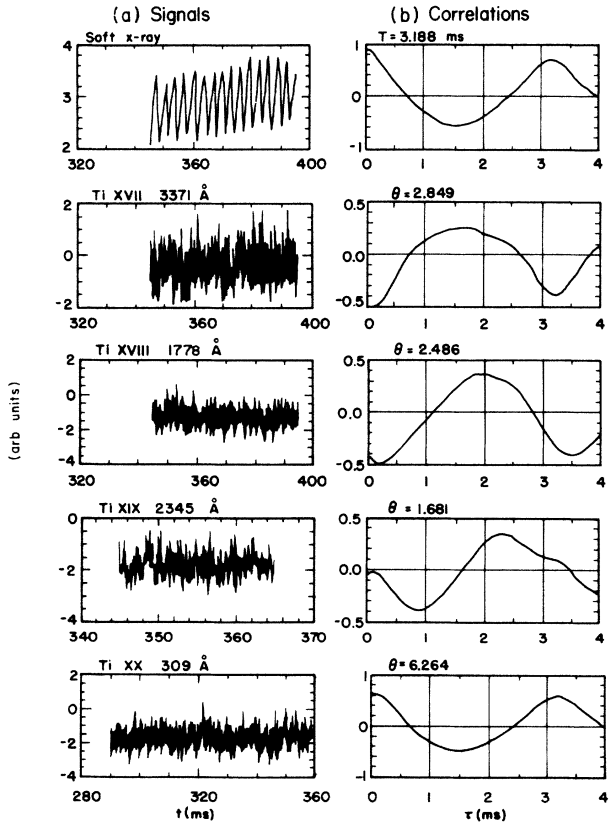

FIG. 2. Signals and correlations for case II. Ti XIX and Ti XX signals are from different shots. T and θ are as in Fig. 1.

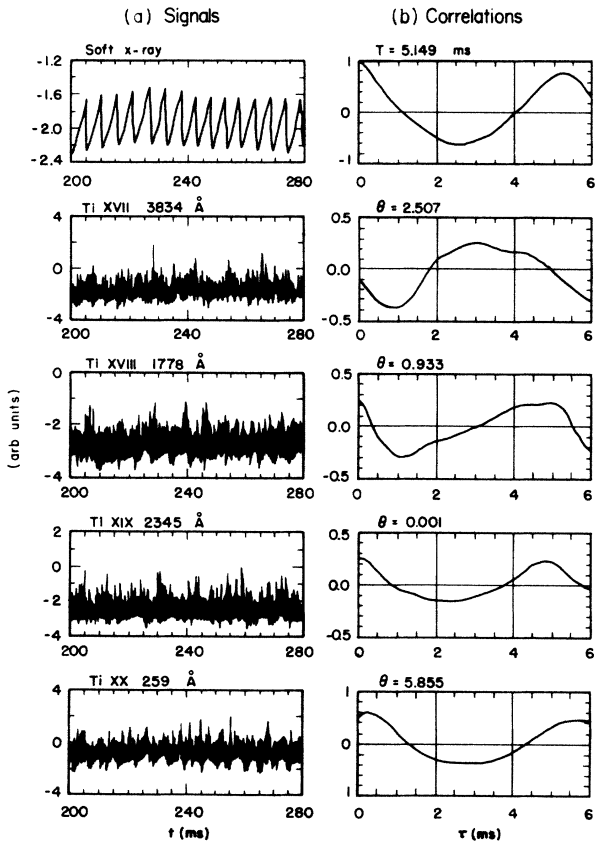

FIG. 3. Signals and correlations for case III. T and θ are as in Fig. 1.

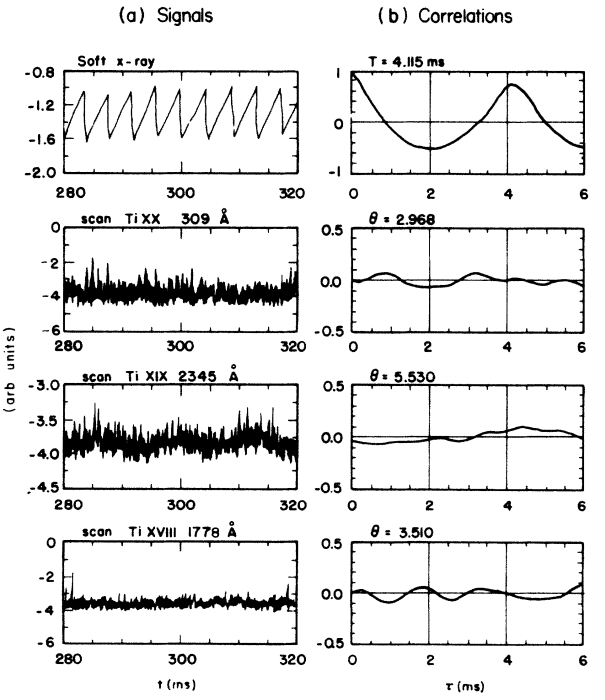

FIG. 4. Correlations and background radiations.

near Ti XX 309 Å, Ti XIX 2345 Å, and Ti XVIII 1778 Å. We also note that the phase shifts for background radiation vary randomly from shot to shot. Totally correlated signals should give an amplitude of ~ 1, as is seen in the autocorrelation of the soft-x-ray signal, e.g., in Fig. 1(b). Even though the correlations for the line signals are less than 1 in Figs. 1(b), 2(b), and 3(b), they clearly show phase shifts relative to the autocorrelations of the soft-x-ray signal. In addition, the correlation functions for Ti XVII, XVIII, XIX, and XX do exhibit distinctly different phase shifts relative to each other. The phase shifts are reproducible to within 0.3 rad or less from shot to shot. These correlation functions are now used for comparison with a computer simulation of the ionization-recombination and ion transport processes in the plasma.

The fractional modulation of the line intensities is small, $\lesssim 5\%$, consistent with the assumption underlying the following analysis that the total titanium distribution is not significantly perturbed by the sawteeth.

IV. NUMERICAL METHOD

Several algorithms have been devised to solve the 1D transport-ionization-recombination equations.[30–32] The algorithms usually involve a division of the spatial dimension into mesh points, conversion of the differential equations into difference equations for quantities on the mesh points, and solving the difference equations. The mesh points can be equidistant, or of varying distances depending especially on the phenomena near the plasma edge. Most of these algorithms require inversions of matrices of dimension either of the number of ionization stages or of the number of mesh points.[30,31] The computer time needed for such inversions is quite long, especially for small computers, i.e., a PDP-11. To reduce the computer time, an algorithm discussed by Lackner *et al.*[32] was used which does not involve matrix inversions.

Here is a brief description of this algorithm. A more detailed discussion and analysis of stability of the algorithm can be found in Lackner *et al.*[32] The difference equations corresponding to Eq. (3) are written as

$$\frac{n_k^{l+1}-n_k^l}{\Delta t}+n_e I_k^{l+1} n_k^{l+1}-n_e I_{k-1}^{l+1} n_{k-1}^{l+1}$$

$$=-\frac{1}{r}\frac{\partial}{\partial r}(r\Gamma^l)+n_e(R_{k+1}^l n_{k+1}^l-R_k^l n_k^l)\,, \quad (7)$$

where superscript l represents the lth time step and subscript k represents the kth ionization stage. The diffusion term is represented by the Crank-Nichelson scheme.[33] The ionization terms are treated implicitly. This allows the use of rather large time steps. Much smaller time steps would be needed if one were to treat ionization explicitly because ionization rates of lower ionization stages are large.

To solve the set of difference equations, one starts from the lowest ionization stage. Because the ionization terms are treated implicitly, the last term on the left-hand side (lhs) of Eq. (7) does not exist for the lowest ionization stage. The solution for each ionization stage is entered

into the third term on the lhs of Eq. (7), as well as the solution from the previous time step, as input for the equations for the next ionization stage. For each ionization stage, the equations are a tridiagonal system in the mesh points, which can be easily solved.[33]

The input parameters needed for solving the equations are the $T_e(r)$-dependent ionization and recombination rate coefficients at each mesh point, the diffusion coefficients, the convective velocities, and the electron density profile $n_e(r)$.

The electron density profile in TEXT is measured by a multichannel microwave interferometer. The electron density profile can be fitted by the form

$$n_e(r)=n_e(0)\{0.9[1-(r/a)^2]+0.1\} ,$$

where $a=27$ cm is the minor radius. The electron temperature in TEXT is measured by Thomson scattering and electron cyclotron emission (ECE). The average electron temperature profile measured by Thomson scattering can be fitted by the form

$$T_e(r)=T_e(0)\exp[-(r/b)^c] ,$$

where $T_e(0)$, b, and c are listed in Table I. Figures 5 and 6 show the electron temperature profile evolution, during the sawtooth oscillation, assumed in our simulation. The electron temperature profile evolution was chosen to be consistent with the soft-x-ray emission profile, especially during the rising phase of the sawtooth oscillation.[34] The declining phase is less important because of its short time. Measurement of electron temperature profile evolution by ECE was not done at the time of our experiment; however, the assumed electron temperature profile evolution is consistent with recent measurement by ECE.

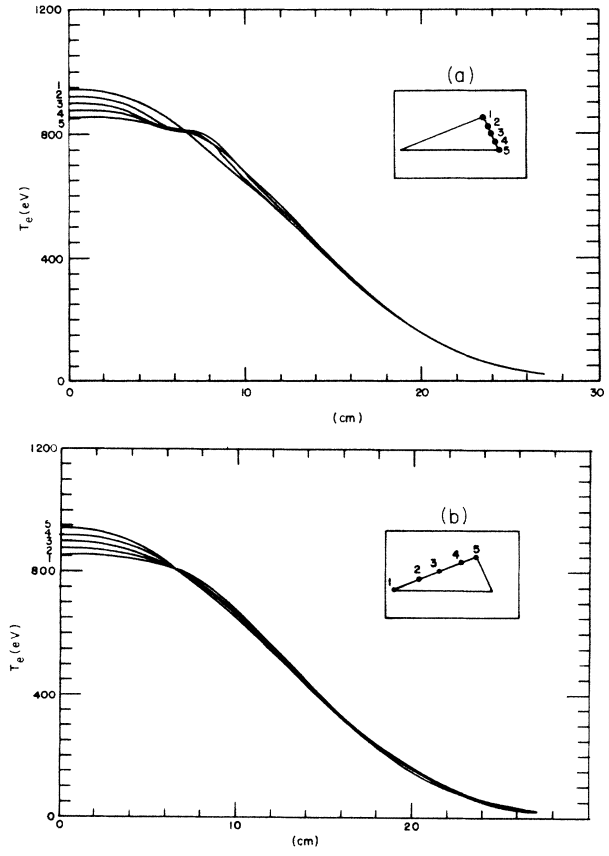

FIG. 5. Electron temperature profile evolution for case I during one sawtooth oscillation. The inserts indicate the time during fall (a) and rise (b) of the sawtooth.

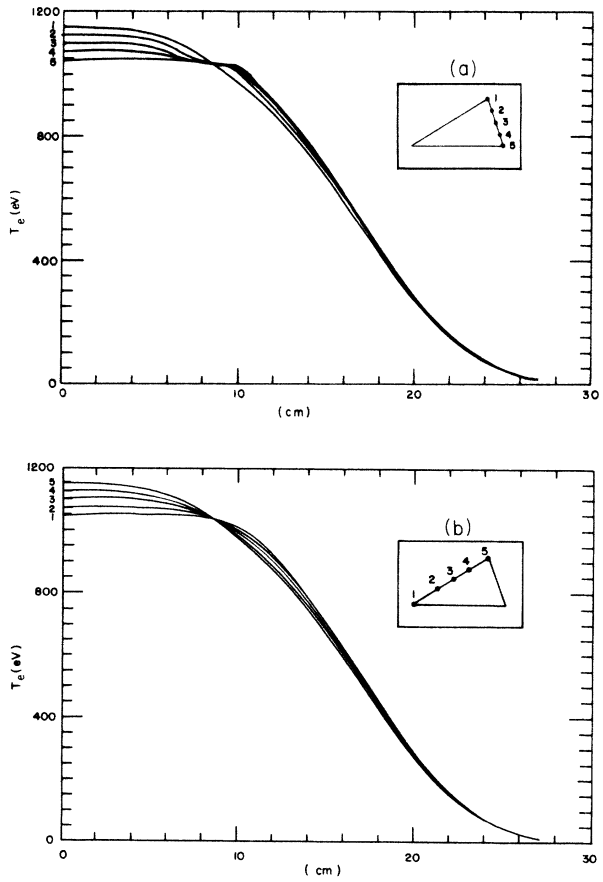

FIG. 6. Electron temperature profile evolution for case II during one sawtooth oscillation. The inserts are as in Fig. 6.

From the electron temperature profile, one can calculate the atomic rate coefficients at each spatial point. The ionization rate coefficients are calculated from Lotz's semiempirical formula.[18] The radiative recombination rate coefficients are approximately evaluated by the hydrogenic formula[35]

$$\alpha^r = 5.0\times 10^{-14} z^4 \left[\frac{I_H}{T_e}\right]^{3/2} \times \left[\frac{1-\zeta/2n_0^2}{n_0^3}\exp\left[\frac{z^2 I_H}{n_0^2 T_e}\right] E_1\left[\frac{z^2 I_H}{n_0^2 T_e}\right] + \sum_{n=n_0+1}^{n_{\max}} \frac{1}{n^3}\exp\left[\frac{z^2 I_H}{n^2 T_e}\right] E_1\left[\frac{z^2 I_H}{n^2 T_e}\right]\right] , \quad (8)$$

where n_0 is the principal quantum number of the outer

main shell, ζ is the number of bound electrons in the shell, I_H is the ionization energy of hydrogen, z is the charge of the recombining ion, n_{max} is chosen to be 25 (since the contribution from higher n is proportional to n^{-3}, the value of n_{max} is not important), and the function E_1 is the exponential integral of index 1. The dielectronic recombination rate coefficients are calculated from Burgess's formula.[19] The transitions, their oscillator strengths, and energies for the calculation of dielectronic recombination rates are listed in Appendix A. The recombination rate coefficients are obtained by adding the dielectronic and radiative rate coefficients. However, the dielectronic rates are much larger than the radiative rates for most ions except Ti XXI. Each rate coefficient is multiplied by an adjustable factor in our code.

The diffusion coefficient is assumed to be independent of radius and ion species. The convective velocity is assumed to have a radial dependence of

$$V(r)=V(a)\frac{r}{a},$$

where $a=27$ cm is the minor radius. The constant diffusion coefficient D and the convective velocity, $V(a)$, of impurity ions were obtained in the TEXT tokamak by the laser blow-off technique.[23] From this measurement, Rowan *et al.* obtained $D\approx 10^4$ cm^2/sec and $V(a)\approx 1000$ cm/sec. These values were used in our code. A 100% recycling of impurities is assumed at the boundary $r=a$. The recycling of impurities is consistent with the fact that the impurity levels remain constant during the quiescent state of the plasma. The time step, Δt in Eq. (7), was chosen to be in the range of 0.01—0.1 ms.

V. THE IONIZATION AND RECOMBINATION RATE COEFFICIENTS

The titanium ions Ti XVII—XX are most abundant in the central region of the plasma, where lower titanium ions are virtually absent. Therefore, the assumed rate coefficients for lower ions do not significantly affect the relative abundances of Ti XVII, XVIII, XIX, and XX, even though they certainly determine the distribution of lower ions near the plasma edge. Thus, only the ionization rate for Ti XVI, the ionization and recombination rates for Ti XVII—XX, and the recombination rate for Ti XX were varied for a best fit to the experimental data.

In the comparison of the simulated results with the experiment, certain criteria were used. The simulated correlations cannot perfectly match the experimental correlations, which are influenced strongly by experimental noise. Though the exact shapes of the correlations are different, nodes, maxima and minima were used as indices for the comparison. The chosen criterion was to match these index points to within 0.2 msec, which corresponds to about a 0.3-rad shift. Such a procedure depends mostly on the accuracy of the measurement of line emission.

The ionization and recombination rate coefficients giving the best match are listed in Table III. Table III also shows the diffusion coefficients and convective velocities used for each plasma condition. Figure 7 shows the correlation functions that are best matched. In Fig. 7 the dotted curves are simulated correlations and the solid curves are experimental correlations.

The electron temperatures listed in Table III are the peak electron temperatures at $r=0$ cm. Since not all ionic abundance profiles are peaking at $r=0$ cm, the listed rates in Table III are only more or less representative. However, the multiplication factors in parentheses are applicable at all radii. The profiles of Ti XIX and XX are peaking at $r=0$ cm for all three conditions. For case III, profiles of Ti XVII and XVIII are also peaking at $r=0$ cm. For case I, Ti XVII and XVIII are peaking at 12 cm ($T_e\sim 600$ eV) and 9 cm ($T_e\sim 700$ eV), respectively. For case II, Ti XVII and XVIII are peaking at 15 cm ($T_e\sim 700$ eV) and 13 cm ($T_e\sim 800$ eV), respectively.

TABLE III. (a) Ionization rate coefficients (10^{-11} cm^{3}sec^{-1}). The numbers in parentheses are multiplication factors for ionization rates calculated by Lotz's formula. (b) Recombination rate coefficients (10^{-12} cm^{3}sec^{-1}). The numbers in parentheses are multiplication factors for calculated recombination rates. (c) Transport parameters used in simulations.

Plasma conditions	T_e (eV)	Ti XVII	Ti XVIII	Ti XIX	Ti XX
		(a)			
I	900	5.5 (1.2)	3.2 (1.2)	1.4 (1.0)	0.8 (1.4)
II	1100	7.7 (1.2)	4.5 (1.2)	2.0 (1.0)	1.0 (1.2)
III	600	2.5 (1.2)	1.4 (1.2)	0.6 (1.0)	0.3 (1.4)
		(b)			
I	900	2.8 (0.8)	6.9 (0.8)	7.0 (0.8)	5.6 (0.8)
II	1100	2.2 (0.8)	5.6 (0.8)	5.8 (0.8)	4.6 (0.8)
III	600	7.0 (1.2)	14.1 (1.1)	13.0 (1.0)	9.6 (1.0)

Plasma conditions	(c) Diffusion coefficient (10^4 cm^2/sec)	Convective velocity (10^3 cm/sec)
I	1	1
II	1.5	1
III	1.2	0.8

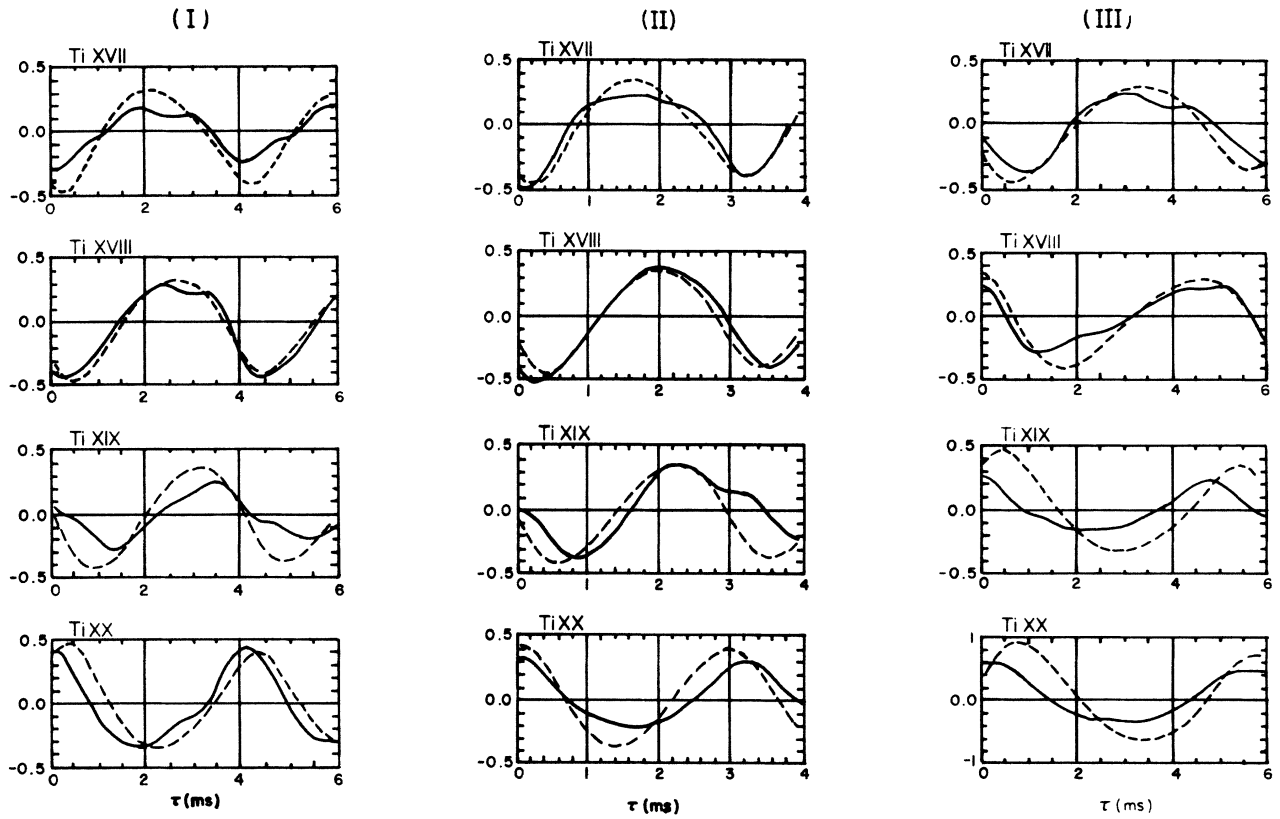

FIG. 7. Best matched normalized correlations (y axis) for cases I–III.

VI. SENSITIVITY ANALYSIS

In order to assess the validity of this method for determining of effective ionization and recombination rate coefficients, several questions must be addressed. Can the rate coefficients be uniquely determined? How accurately can they be determined? How important is the effect of transport? Do the diffusion coefficient and convective velocity have to be known exactly? How does the uncertainty in the electron temperature measurement affect our result? These questions can be answered by a sensitivity analysis of the variation of the various parameters. The sensitivity analysis was done for case I.

A. The rate coefficients

The search for a set of rate coefficents that matches our measurements was subject to the criterion that the measured rate coefficients should not be too different from values of the ionization rate predicted by Lotz's semiempirical formulas[18] and the predictions of Refs. 35 and 19 for radiative and dielectronic recombination. Within this limited parameter space (with multiplication factors from 0.3 to 3) there are no other acceptable sets of coefficients.

To estimate the sensitivity of the analysis, the influence of rate coefficient variations on the correlation was studied. Figures 8 and 9 show the simulated correlations for different sets of rate coefficients. In Fig. 8, (a) the ionization rates for all ions are increased by 30%, (b) the recombination rates are increased by 60%, and (c) both ionization and recombination rates are increased by 40%. In Fig. 9, (a) the ionization rates are reduced by 30%, (b) the recombination rates are reduced by 60%, and (c) both ionization and recombination rates are reduced by 40%. In both Figs. 8 and 9, the solid curves are the best matched correlations. The most significant changes occur when the ionization rates are varied [Figs. 8(a) and 9(a)]. The error of the ionization rate can be estimated to be less than 20%. The correlations are less sensitive to variation of recombination rates [Figs. 8(b) and 9(b)]. The recombination rates can only be determined to be within $\pm 60\%$. Figures 8(c) and 9(c) indicate the range over which absolute values of the rate coefficients may vary while keeping their relative values unchanged. However, the variation of correlations in Fig. 8(c) and 9(c) are mostly due to change of ionization rates.

Changes of rate coefficients for individual ion species can also result in differences in the correlations. Such a change tends to affect the corresponding ion itself and its adjacent ions. The correlation is less sensitive to the recombination rate coefficient for Ti XXI and ionization rate coefficients for Ti XVI. The recombination rate coefficient of Ti XXI was varied by 50% or more with only a small change in the correlations. This can be explained by the fact that this recombination rate coefficient ($\sim 2\times 10^{-12}$ cm^{3}sec^{-1} at 900 eV) is much smaller than the rate coefficients of other ions (see Table III). Any reasonable change in the recombination rate for Ti XXI mostly produces a change in the total abundance of the

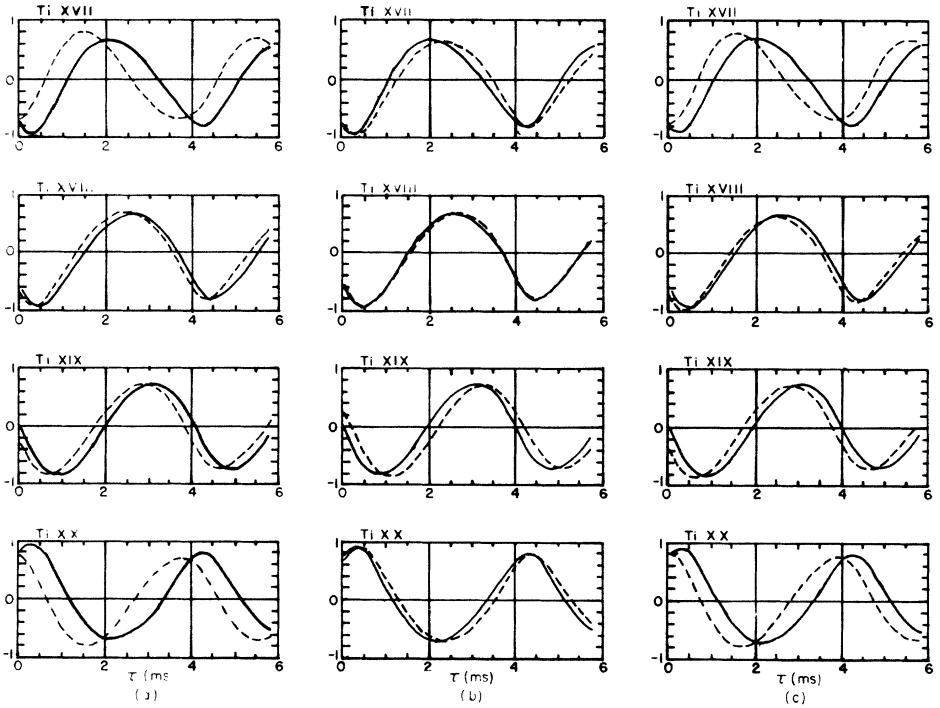

FIG. 8. Variations of the normalized correlations (y axis). (a) All ionization rates are increased by 30%. (b) All recombination rates are increased by 60%. (c) Both ionization and recombination rates are increased by 40%.

lower ions which can adjust their relative abundances on a much faster time scale. Increasing the ionization rate coefficients for Ti XVI by 50% or more did not change the correlations either. This is because Ti XVI is much less abundant so that an increase of its ionization rate does not affect the abundance of the other ions significantly.

B. The effect of transport

Impurity transport is very important for the calculation of radiative energy losses from fusion plasmas. It has been shown that internal disruptions can greatly reduce the concentration of impurities near the center of a tokamak plasma.[22,36] Inward convection, however, increases the confinement time of impurity ions.[37] No ap-

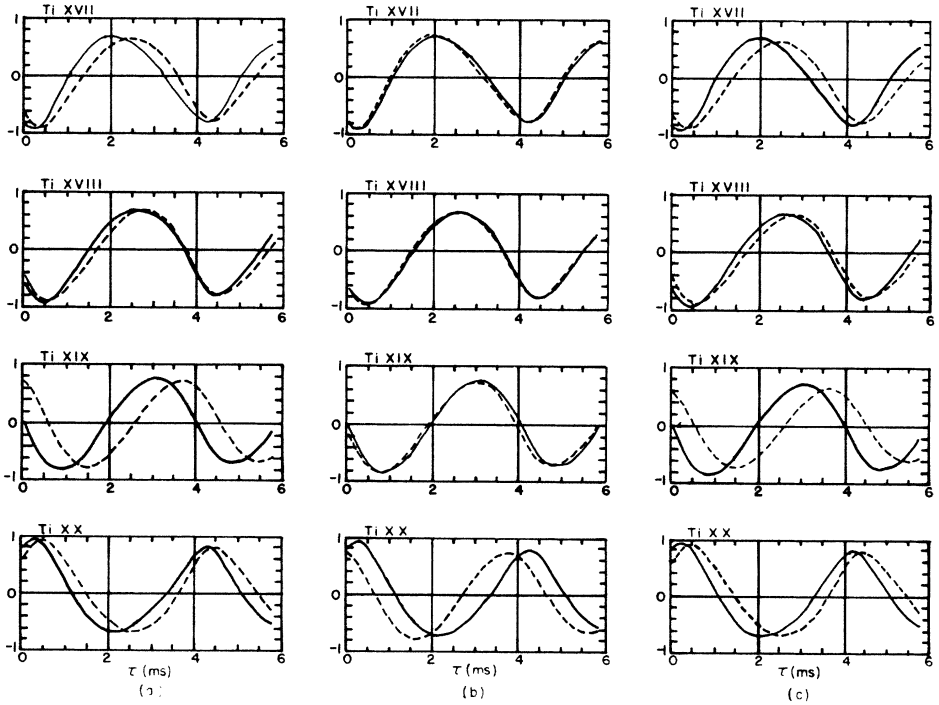

FIG. 9. Variations of the normalized correlations (y axis). (a) All ionization rates are reduced by 30%. (b) All recombination rates are reduced by 60%. (c) Both ionization and recombination rates are reduced by 40%.

preciable effects that may be associated with the uncertainties in the appropriate values of the diffusion coefficients and the convection velocity were found in our experiment. The effects of the assumed transport on the simulated correlations can be seen by varying the diffusion coefficient and the convective velocity. Figure 10 shows the correlations for diffusion coefficients of 5×10^3 and 2×10^4 cm^2/sec, with corresponding changes in the convective velocity to keep the ratio $V(a)/D$ unchanged. The convective velocity was varied from 100 to 2000 cm/sec with fixed diffusion coefficient. The results are shown in Fig. 11. Figure 12 shows correlations with the diffusion coefficient varied from 5000 to 20 000 cm^2/sec, while the convective velocity was 10^3 cm/sec. In Figs. 10–12 the solid curves are the best matched correlations.

As can be seen from Figs. 10–12, the correlation of Ti XVII is most affected by the lowering of the diffusion coefficient. The correlations of all ions are insensitive to the variation of convective velocity and increase in the diffusion coefficient. The results indicate that for ions that are abundant at small radius, Ti XX, XIX, and possibly XVIII, the atomic processes dominate the transport process. Ti XVII, which exists at larger radius, is more affected by diffusion. With small diffusion coefficient, Ti XVII is less abundant near the center of the plasma where atomic processes are most effective. The convective velocity does not have much effect on the correlation because of its linear dependence on the radius r. Since most of the ions concentrate at small radius ($r \leq 15$ cm), the value of convective velocity is also small.

The results show that the transport, except for possible anomalous effects (see Sec. VII), is not critical for the analysis, if the transport coefficients are known to be within a factor of 2. Such a limitation is consistent with the sensitivity of the method with respect to the rate coefficients.

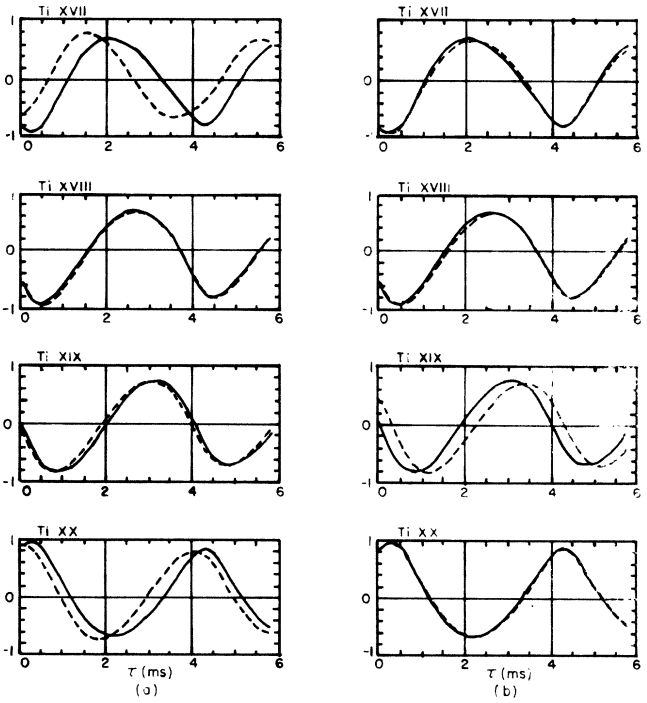

FIG. 10. Variation of normalized correlations (y axis). (a) $D=5\times10^3$ cm^3/sec. (b) $D=2\times10^4$ cm^2/sec. The convective velocity is changed accordingly to keep the ratio $V(a)/D$ fixed.

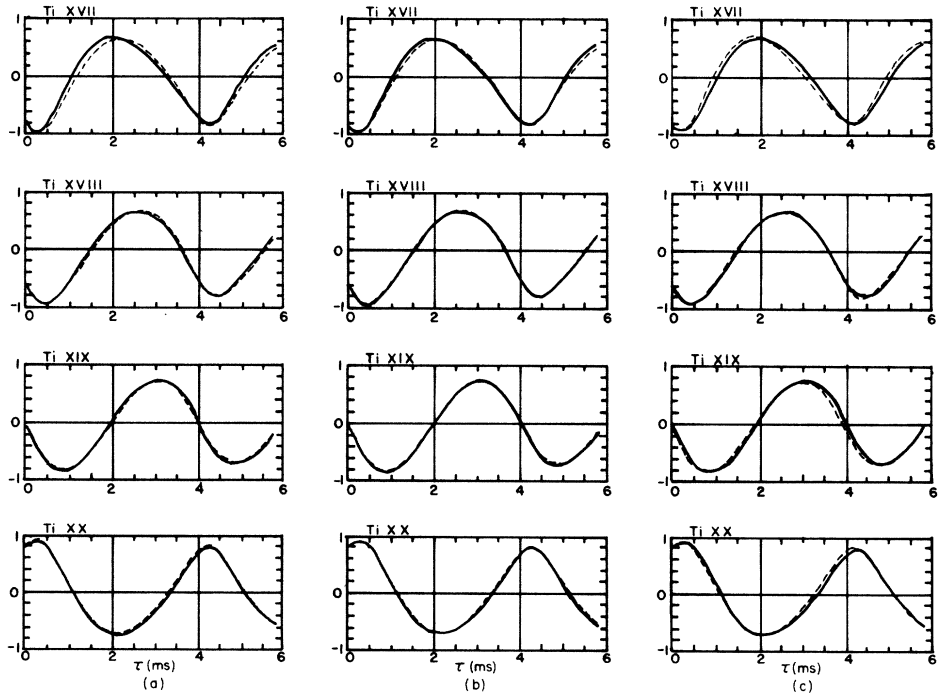

FIG. 11. Variation of normalized correlations (y axis). (a) $V(a)=10^2$ cm/sec. (b) $V(a)=5\times10^2$ cm/sec. (c) $V(a)=2\times10^3$ cm/sec. $D=10^4$ cm^2/sec for (a)–(c).

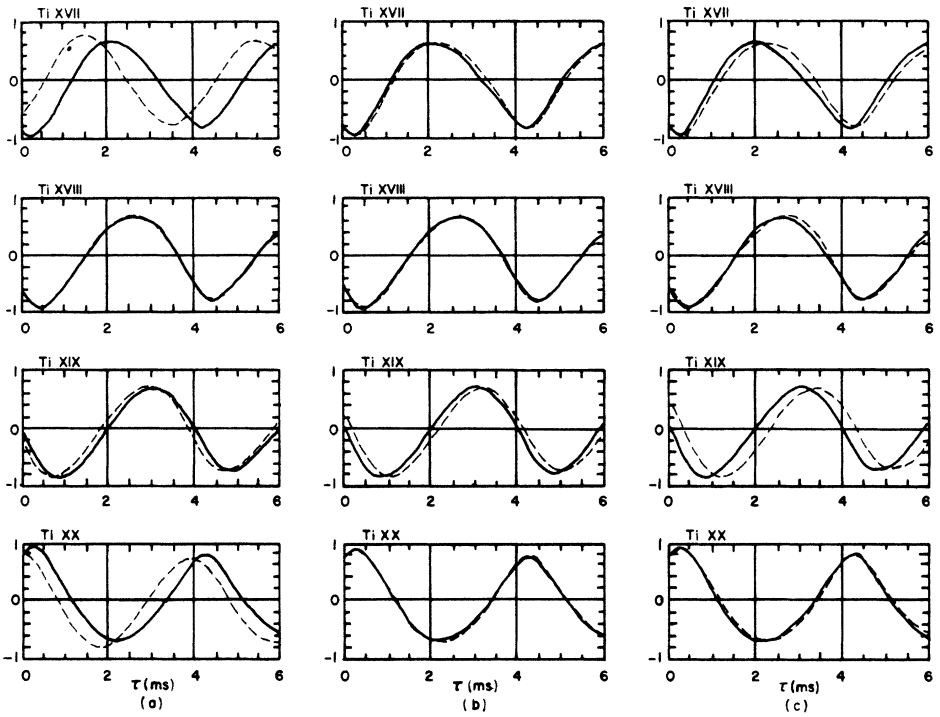

FIG. 12. Variation of normalized correlations (y axis). (a) $D=5\times10^3$ cm^2/sec. (b) $D=1.5\times10^4$ cm^2/sec. (c) $D=2\times10^4$ cm^2/sec. $V(a)=10^3$ cm/sec for (a)–(c).

C. The effect of the amplitude of electron temperature variations

The amplitude of the simulated temperature fluctuation has been varied from 2–20 % of the average to check for any difference in our results. As expected, the amplitudes of modulation of line emissions are different, as the amplitude of the T_e variation changes, but the normalized correlation functions remain unchanged. This may be explained by the fact that the assumed rate coefficients are almost linear functions of T_e at $T_e \approx 900$ eV.

This situation is advantageous because while the variation of electron temperature can be inferred from the soft-x-ray signal its amplitude cannot because the sensitivity of the detector is difficult to calibrate. Ideally, single-shot multipoint Thomson scattering or a tunable electron cyclotron radiometer would provide a better estimate for the variation in central electron temperature. However, such measurements are difficult and errors in measurements may be comparable with ΔT_e.

The average electron temperature in the simulation was varied with the result that the average electron temperature must be known within 50 eV. This is, however, about the accuracy of the Thomson scattering measurement.

VII. DISCUSSION

The ionization rate coefficients we have obtained are about a factor of 1.2 larger than the values calculated by Lotz's formula. A comparison with Younger's calculation, for lithiumlike Ti XX (Ref. 38) and berylliumlike Ti XIX,[39] also shows that our values are a factor of 1.2 larger. The explanation for a possibly higher ionization rate can be twofold. Underestimation of ionization cross sections at threshold can reduce the theoretical values, because the electron temperature is near or less than the ionization potential of the ions. Other processes such as inner-shell excitation followed by autoionization[40] and double ionization[41] can also increase ionization cross sections. Though these effects are negligible at 600–1100 eV, they can enhance the ionization rates in the presence of a high-energy tail in the electron velocity distribution. However, our method for matching the correlations is sensitive to the variation of ionization rates to within 20%.

The experimental recombination rates are within 20% of the theoretical values. For all ions, except Ti XXI, the dielectronic recombination is the dominant process. Thus, Burgess's formula for dielectronic recombination rates is suitable for these ions. A possible explanation for lower values of experimental recombination rates is the overestimation of the probability of stabilizing radiation. Autoionization from levels of the cascading process can reduce the recombination rates.[42] A comparison of our measurement with the calculation of McLaughlin and Hahn[43] shows the recombination rates agree well for Ti XX. However, for Ti XIX the calculation is a factor of 2 larger than our measurement. Since our method is not sensitive to the recombination rate for Ti XXI, one should use the theoretical radiative recombination rate for this ion.

Any effects of large anomalous diffusion during the sawtooth crash (see Sec. II) were neglected in our analysis. However, we found that the fit could be improved for condition III, if the diffusion coefficient was increased by

TABLE IV. Atomic data used in Burgess's formula.

Ion	Transition	Wavelength (Å)	Oscillator strength[a]	Δn
Ti XXI	$1s^2(^1S_0)$-$1s2p(^1P_1)$	2.6101	7.35[−1]	1
	-$1s3p(^1P_1)$	2.23	1.41[−1]	2
Ti XX	$2s(^2S_{1/2})$-$2p(^2P_{1/2})$	309.15	2.12[−2]	0
	-$2p(^2P_{3/2})$	259.30	5.86[−2]	0
	-$3p(^2P_{3/2})$	15.253	1.25[−1]	1
	-$3p(^2P_{1/2})$	15.211	2.43[−1]	1
	-$4p(^2P_{1/2,3/2})$	11.452	4.0[−1]	2
	-$5p(^2P_{1/2,3/2})$	10.278	4.0[−2]	3
	-$6p(^2P_{1/2,3/2})$	9.733	2.11[−2]	4
	-$7p(^2P_{1/2,3/2})$	9.434	1.24[−2]	5
	-$8p(^2P_{1/2,3/2})$	9.246	7.7[−3]	6
Ti XIX	$2s^2(^1S_0)$-$2s2p(^1P_1)$	169.59	1.75[−1]	0
	-$2s2p(^3P_1)$	328.36	6.6[−4]	0
	-$2s3p(^1P_1)$	15.866	6.4[−1]	1
Ti XVIII	$2p(^2P_{3/2})$-$2s2p^2(^2D_{3/2})$	200.18	1.2[−3]	0
	-$2s2p^2(^2D_{3/2})$	197.838	4.0[−2]	0
	-$2s2p^2(^2S_{1/2})$	161.97	1.2[−3]	0
	-$2s2p^2(^2P_{1/2})$	147.607	4.07[−2]	0
	-$2s2p^2(^2P_{3/2})$	144.759	9.89[−2]	0
	-$2s2p^2(^4P_{1/2})$	397.6	7.7[−5]	0
	-$2s2p^2(^4P_{3/2})$	363.7	4.7[−5]	0
	-$2s2p^2(^4P_{5/2})$	330.6	3.5[−4]	0
	-$2s^23s(^2S_{1/2})$	18.38	2.0[−2]	1
	-$2s^23d(^2D)$	17.39	2.0[−2]	1
	-$2s^23d(^2D_{5/2})$	17.36	0.58	1
	-$2s^24s(^2S_{1/2})$	13.45	4.3[−3]	2
	$2p(^2P_{1/2})$-$2s2p^2(^2D_{3/2})$	179.902	6.11[−2]	0
	-$2s2p^2(^2S_{1/2})$	148.438	8.37[−2]	0
	-$2s2p^2(^2P_{1/2})$	136.28	1.41[−2]	0
	-$2s2p^2(^2P_{3/2})$	133.852	2.77[−2]	0
	-$2s2p^2(^4P_{1/2})$	324.9	3.0[−4]	0
	-$2s2p^2(^4P_{3/2})$	301.9	1.2[−5]	0
	-$2s^23s(^2S_{1/2})$	18.19	2.0[−2]	1
	-$2s^23d(^2D_{3/2})$	17.22	6.5[−1]	1
	-$2s^24s(^2S_{1/2})$	13.35	4.5[−3]	2

a factor of 5 during the crash of the sawtooth oscillations. This is not true for the other two conditions. Conditions I and II have worse fits when the diffusion coefficient is increased during the declining phase.

Since the amplitude of the sawtooth oscillations of condition III is larger than for the other two conditions, it is conceivable that the anomalous diffusion exists only for this condition. Although such anomaly in the transport processes may affect the line emission time history, we think it only plays a minor role as already shown in our analysis.

ACKNOWLEDGMENTS

We wish to thank K. W. Gentle, TEXT Director, for his cooperation during this experiment; R. V. Bravenec, Burton Richards, and Kjell Nelin for operating TEXT; P. E. Phillips for Thomson scattering data; D. M. Patterson for provision of data acquisition and archiving; and the members of the TEXT Technical Staff for assisting in set-up. This work was supported by the U.S. Department of Energy.

APPENDIX: DIELECTRONIC RECOMBINATION RATE COEFFICIENTS

The dielectronic recombination rate coefficients for titanium ions are calculated by Burgess's formula[19]

$$\alpha^d = 2.4\times 10^{-9}(kT_e)^{-3/2}B(z) \times \sum_j \bar{f}_{j_0 j} A(x)\exp(-E/kT_e) ,$$

TABLE IV. (*Continued*).

Ion	Transition	Wavelength (Å)	Oscillator strength[a]	Δn
Ti XVII	$2s^22p^2(^3P_2)$-$2s\,2p^3(^3D_2)$	191.16	4.8[−4]	0
	-$2s\,2p^3(^3D_1)$	190.17	5.0[−5]	0
	-$2s\,2p^3(^3D_3)$	188.312	3.9[−2]	0
	-$2s\,2p^3(^3P_1)$	159.955	8.5[−3]	0
	-$2s\,2p^3(^3P_2)$	158.469	5.1[−2]	0
	-$2s\,2p^3(^3S_1)$	127.782	6.8[−2]	0
	-$2s\,2p^3(^1D_2)$	126.676	7.2[−3]	0
	-$2s^2p^2(^5S_2)$	364.0	1.6[−4]	0
	$2s^22p^2(^2P_1)$-$2s\,2p^3(^3D_2)$	182.072	5.5[−2]	0
	-$2s\,2p^3(^3D_1)$	181.67	6.3[−3]	0
	-$2s\,2p^3(^3P_0)$	154.133	1.94[−2]	0
	-$2s\,2p^3(^3P_1)$	153.554	3.00[−2]	0
	-$2s\,2p^3(^3P_2)$	152.174	6.0[−3]	0
	-$2s\,2p^3(^3S_1)$	123.654	5.2[−2]	0
	-$2s\,2p^3(^1P_1)$	109.432	3.9[−3]	0
	-$2s\,2p^3(^5S_2)$	332.4	1.6[−4]	0
	$2s^22p^2(^3P_0)$-$2s\,2p^3(^2D_1)$	172.380	8.6[−2]	0
	-$2s\,2p^3(^3P_1)$	146.856	3.68[−2]	0
	-$2s\,2p^3(^3S_1)$	119.284	5.1[−2]	0
	$2s^22p^2(^1S_0)$-$2s\,2p^3(^1P_1)$	142.589	1.23[−1]	0
	$2s^22p^2(^1D_2)$-$2s\,2p^3(^1D_2)$	141.948	1.17[−1]	0
	-$2s\,2p^3(^3D_1)$	227.57	2.9[−4]	0
	-$2s\,2p^3(^3D_3)$	224.16	3.4[−3]	0
	-$2s\,2p^3(^3P_1)$	185.1	6.0[−4]	0
	-$2s\,2p^3(^3P_2)$	183.11	5.6[−4]	0
	-$2s^22p\,3s(^1P_1)$	19.718	4.2[−2]	1

[a]The negative integers give the power of 10 of the multipliers of the numbers listed.

where

$$E=\Delta E_{j_0 j}/a\ ,$$

$$a=1+0.015z^3/(z+1)^2\ ,$$

$$B(z)=[z^{1/2}(z+1)^{5/2}]/(z^2+13.4)^{1/2}\ ,$$

$$A(x)=x^{1/2}/(1+0.105x+0.015x^2)\ ,$$

$$x=\Delta E_{j_0 j}/I_{\rm H}(1+z)\ .$$

Here $\Delta E_{j_0 j}$ and $f_{j_0 j}$ are the excitation energy and oscillator strength. $I_{\rm H}$ is ionization energy of hydrogen atom and z is charge of the recombining ion. However, if the ground configuration has more than one level (i.e., Ti XVIII), one has to average ΔE and f over the ground levels. We assume that in our calculation the ground levels are populated according to their statistical weight g_i. Such an assumption may not be true when the radiative transitions between ground levels have rates comparable to the collisional excitation rates. For $\Delta n\neq 0$,[44] we use

$$A(x)=0.5x^{1/2}/(1+0.210x+0.030x^2)\ .$$

The transitions and their oscillator strengths[45] that we have used to calculate the dielectronic recombination rate coefficients for Ti XVII–TiXXI are listed in Table IV.

[1]H.-J. Kunze, Space Sci. Rev. **13**, 565 (1972).

[2]R. L. Brooks, R. U. Datla, and H. R. Griem, Phys. Rev. Lett. **41**, 107 (1978).

[3]R. L. Brooks, R. U. Datla, A. D. Krumbein, and H. R. Griem, Phys. Rev. A **21**, 1387 (1980).

[4]C. Breton, C. DeMichelis, M. Finkenthal, and M. Mattioli, Phys. Rev. Lett. **41**, 110 (1978).

[5]R. C. Isler, E. C. Crume, and D. E. Arnarius, Phys. Rev. A **26**, 2105 (1982).

[6]B. N. Chichkov, M. A. Mazing, A. P. Shevelko, and A. M. Urnov, Phys. Lett. **83A**, 401 (1981).

[7]F. Bely-Dubau *et al.*, Phys. Lett. **93A**, 189 (1983).

[8]M. Bitter *et al.*, Phys. Rev. A **29**, 661 (1984).

[9]S. von Goeler, W. Stodiek, and N. Sauthoff, Phys. Rev. Lett. **33**, 1201 (1974).

[10]F. Korgar, *et al.*, in *Plasma Physics and Controlled Nuclear*

Fusion Research, Proceedings of the Sixth Conference, Berchtesgaden, 1976 (IAEA, Vienna, 1977), Vol. I, p. 267.
[11]G. Jahns, M. Soler, B. V. Waddell, J. D. Callen, and H. R. Hicks, Nucl. Fusion **18**, 609 (1978).
[12]M. A. Dubois, A. L. Peiquet, and C. Reverdin, Nucl. Fusion **23**, 147 (1983).
[13]N. H. Brooks, Phys. Fluids **20**, 711 (1977).
[14]E. Hinnov *et al.*, Bull. Am. Phys. Soc. **25**, 902 (1980).
[15]TFR Group, Plasma Phys. **19**, 349 (1977).
[16]R. W. P. McWhirter, in *Plasma Diagnostic Techniques,* edited by R. H. Huddelstone and S. L. Leonard (Academic, New York, 1965), p. 201.
[17]A. K. Bhatia, U. Feldman, and G. A. Doschek, J. Appl. Phys. **51**, 1464 (1980).
[18]W. Lotz, Institut für Plasmaphysik, Garching bei München, Report No. IPP 1/62, 1978 (unpublished).
[19]A. Burgess, Astrophys. J. **141**, 1588 (1965).
[20]W. D. Stanley, *Digital Signal Processing* (Reston, Reston, VA, 1975).
[21]R. Petrasso, F. H. Segnin, N. G. Loter, E. Marmar, and J. Rice, Phys. Rev. Lett. **49**, 1826 (1982).
[22]TFR Group, Nucl. Fusion **25**, 981 (1985).
[23]W. L. Rowan *et al.*, Bull. Am. Phys. Soc. **28**, 1033 (1983).
[24]K. W. Gentle, Nucl. Technol./Fusion **1**, 479 (1983).
[25]T. P. Kochanski, T. Boyd, J. A. Snipes, and S. R. Kim, Bull. Am. Phys. Soc. **27**, 829 (1982).
[26]K. D. Lawson, N. J. Peacock, and M. F. Stamp, J. Phys. B **14**, 1929 (1982).
[27]E. Hinnov, Astrophys. J. **230**, L197 (1979).
[28]S. Suckewer, R. Fonck, and E. Hinnov, Phys. Rev. A **21**, 924 (1980).
[29]*Programs for Digital Signal Processing,* edited by the Digital Signal Processing Committee, IEEE Acoustics, Speech, and Signal Processing Society (IEEE, New York, 1979).
[30]R. A. Hulse, Nucl. Technol./Fusion **3**, 259 (1983).
[31]M. Okamoto and T. Amano, J. Comput. Phys. **26**, 80 (1978).
[32]L. Lackner, K. Behringer, W. Engelhardt, and R. Wunderlich, Z. Naturforsch. **37A**, 931 (1982).
[33]D. Potter, *Computational Physics* (Wiley, New York, 1973).
[34]J. A. Snipes, T. P. Kochanski, and S. B. Kim, The University of Texas Fusion Research Center Report No. 225, August, 1983 (unpublished).
[35]H. R. Griem, *Plasma Spectroscopy* (McGraw-Hill, New York, 1964), p. 160.
[36]G. L. Jahns *et al.*, Nucl. Fusion **22**, 1049 (1982).
[37]K. H. Burrell *et al.*, Nucl. Fusion **21**, 1009 (1981).
[38]S. M. Younger, Phys. Rev. A **22**, 111 (1980).
[39]S. M. Younger, Phys. Rev. A **24**, 1278 (1981).
[40]A. Burgess and M. C. Chidichimo, Mon. Not. R. Astron. Soc. **203**, 1269 (1983).
[41]M. S. Pindzola *et al.*, Phys. Rev. A **29**, 1749 (1984).
[42]M. Blaha (private communication).
[43]D. J. McLaughlin and Y. Hahn (private communication).
[44]A. L. Merts, R. D. Cowan, and N. J. Magee, Jr., Los Alamos Scientific Laboratory Report No. LA-6220-MS, 1976 (unpublished).
[45]Kazyo Mori, Japan Atomic Energy Research Institute Report No. JAERI-M 82-078, 1982 (unpublished).